RSC Advances

Self-assembled tubular nanostructures of tris(8-quinolinolato)gallium(III)

Journal:	*RSC Advances*
Manuscript ID:	RA-COM-07-2015-014452.R2
Article Type:	Communication
Date Submitted by the Author:	04-Sep-2015
Complete List of Authors:	Xie, Wanfeng; Shandong University, School of Physics Wang, Fenggong; University of Maryland, Materials Science and Engineering Department Fan, Jihui; Shandong University, School of Physics Song, Hui; Shandong University, School of Physics Wu, Zongyong; Shandong University, School of Physics Yuan, Huimin; Shandong University, School of Physics Jiang, Feng; Shandong University, School of Physics Pang, Zhiyong; Shandong University, School of Physics Han, Shenghao; Shandong university, School of Physics

RSC Advances

COMMUNICATION

Self-assembled tubular nanostructures of tris(8-quinolinolato)gallium(III)

Received 00th July 2015,
Accepted 00th January 2015

DOI: 10.1039/x0xx00000x

www.rsc.org/advances

Wanfeng Xie,[a] Fenggong Wang,[c] Jihui Fan,[a] Hui Song,[a] Zongyong Wu,[a] Huimin Yuan,[a] Feng Jiang,[a] Zhiyong Pang,*[a] and Shenghao Han*[ab]

We report for the first time the controllable growth of tubular nanostructures at the nanoscale of the broadly applied organic drug material, tris(8-hydroxyquinoline)gallium (Gaq_3), by an extremely facile approach. The products show a relatively low turn-on field (8.5 V um^{-1}) and a very high maximum current density (2.3 mA cm^{-2}). The length of the Gaq_3 tubes and nanostructures can be readily manipulated and the adopted method is highly transferrable to other organic materials.

Introduction

When material's either dimension reaches nanoscale (<100 nm), lots of exotic phenomena unobservable in bulk arise, accompanying by atomic-scale structural changes at or near surfaces or interfaces.[1-5] This has triggered enormously promising applications of nanomaterials, ranging from nanooptoelectronics, nanophotonics, and nanocatalytics to other energy, environmental, and biomedical applications.[6-10] Organic nanomaterials, bridging organics and nanoscience, are especially interesting in terms that they have a strong diversity, giving rise to an advantage for interdisciplinary applications.[3,5,11-15] In addition, the shape and structure of materials can significantly affect their functional properties, which is mostly evident in carbon allotropes and from the importance of materials' surface-volume ratio in optoelectronics, photovoltaics, and photocatalytics.[4,10,16,17] Therefore, there has been a great desire for controllable growth of organic nanomaterials with particular shapes and structures.

The 8-hydroxyquinoline metal chelates (Mq_3, M=Al and Ga), as typical organic materials, are widely used in physical, chemical, biological, and pharmaceutical applications,[18-22] including but not limited to organic light-emitting diodes (OLEDs),[18] panel displays,[19] spin valves,[20]anticancer drugs,[21-23] and sensors.[24] Compared to Alq_3, Gaq_3 finds its superiority towards real-world applications. For example, Gaq_3-based OLED devices possess a lower turn-on voltage,[19] leading to a proportionally higher power efficiency.[19,25-28] In addition, Gaq_3 is a more promising therapeutic material due to its limited solubility in water.[23] This has been demonstrated by the recent successes of Gaq_3 in phase I clinical trials, where it shows a strong activity against renal cell cancer.[23,29-32] To the best of our knowledge, however, less attention has been concentrated on the research of the fabrication and characterizations of Gaq_3 material with novel nanostructures.[33-36] Tubular especially the tube-in-tube and rod-in-tube nanostructures are of special interest because they have greater tunability or higher surface-volume ratio.

While emphasizing the great implications of controllable growth of nanomaterials with desired shapes, here we report the successful synthesis of Gaq_3 tubular nanostructures by an extremely facile solution method. Tube-in-tube and rod-in-tube nanostructures are achieved during the growth process. We show that these tubular nanostructures possess outstanding optical especially field-emission properties. In addition, this growth is done at room temperature without any exterior assistant and the adopted method is highly transferable to other organic materials.

Experimental

Materials: Commercial Gaq_3 powders are provided by the Nichem company while Chloroform ($CHCl_3$) and ethanol (C_2H_6O) are supplied by the Tianjin Fuyu Fine Chemical Co., Ltd.

Synthesis of Gaq_3 sub-microtubes: Initially, Gaq_3 solution was prepared by using only the Gaq_3 powder and organic mixture solvent. At first, a certain amount of Gaq_3 powders and

[a] School of Physics, State Key Laboratory of Crystal Materials, Shandong University, Jinan 250100, P. R. China.

[b] China.hansh@sdu.edu.cn; pang@sdu.edu.cn; Tel & Fax: +86 531 88365435

[c] School of Space Science and Physics, Shandong University, Weihai 264209, P. R. China

[d] Materials Science and Engineering Department, University of Maryland, College Park, Maryland 20910, United States.

† Footnotes relating to the title and/or authors should appear here.
Electronic Supplementary Information (ESI) available: Detailed descriptions of experimental methods, synthetic procedures, characterization of the Gaq_3nanostructres and additional SEM images. See DOI: 10.1039/x0xx00000x

the solvent were mixed together, followed by an agitation process by magnetic stirrer for 12 hours. Then, a little of evenly-mixed Gaq_3 stock solution was dropped slowly onto the silicon substrates. After two days, the Gaq_3 sub-microtubes formed on a large scale on the substrates due to the volatilization of $CHCl_3$ at room temperature.

The microstructure analysis of crystalline Gaq_3 sub-microtubes was carried out on a Powder X-Ray Diffraction (XRD, Bruker AXS, D8 Advance) and Fourier transform infrared spectroscopy (Thermo Nicolet, NEXUS 670). The surface morphology and size of the as-prepared Gaq_3 sub-microtubes were characterized by a high resolution Scanning Electron microscope (SEM, S-4800) and transmission electron microscopy (TEM, Tecnai G^2 F20). The photoluminesence (PL) signal from the samples was dispersed by a Jobin-Yvon iHR320 monochromator excited at 325 nm and detected by a thermoelectrical cooled Synapse CCD detector. The absorption spectrum was measured by a UV-Vis spectrophotometer (U-4100). Field emission measurements were performed in a vacuum chamber of 5×10^{-7} Pa at room temperature under a two-parallel-plate configuration.

Results and discussion

A bunch of as-prepared Gaq_3 sub-microtubes have successfully been fabricated by this approach. These sub-microtubes possess relatively high monodispersity, uniform shapes, similar sizes, and smooth surfaces at the entire length scale, evident from the low resolution scanning electron microscope (SEM) image (Fig. 1A). The SEM images with higher resolution (Fig. 1B, 1C and 1D) further reveal that these sub-microtubes are in hexagonal hollow structures, with an aspect ratio of ~3.5, diameter of ~4 um and length of ~14 um. Their terminating surfaces are uneven (Fig. 1B), similar to what found for the self-assembled hollow 2,4,5-triphenylimidazole (TPI) sub-microtubes and Porphyrin nanoprisms.[12,37] In addition, the cross sections of these tubes are all in square-like shapes (see Fig. 1C and 1D), which is very different from previous experiment that a circular cross section is typically observed for the tubular structures of other organic or inorganic materials.[38,39] The hollow nature of these tubular structures is further confirmed by the transmission electron microscope (TEM) (Fig. S1†). The wall thickness is at the nanoscale, typically less than 200 nm (Fig. 1D). Additionally, the molecular nature of these tubes can be corroborated by the detailed energy-dispersive spectroscopy (EDS) analysis (Fig. S2†), which shows peaks of C, O, N and Ga elements ($C_{27}H_{18}GaN_3O_3$). The hollow hexagonal prismatic morphology observed by SEM suggests that these material samples belong to the α-crystalline phase, confirmed by the Fourier transform infrared spectroscopy (FTIR) and powder X-ray diffraction (XRD) (Fig. S3†) analyses. The FTIR peak at 408 cm^{-1} is ascribed to the Ga-N stretching vibrational mode, while the peaks at 522.9 and 742.5 cm^{-1} corresponding to the Ga-O stretching vibration mode, all in good agreement with previous literature.[27,40] Therefore, we have successfully synthesized tubular Gaq_3 nanostructures with nanoscale wall thickness, and in the following we explore the growth mechanism and look into how controllable growth of nanomaterials with different shapes and structures can be achieved.

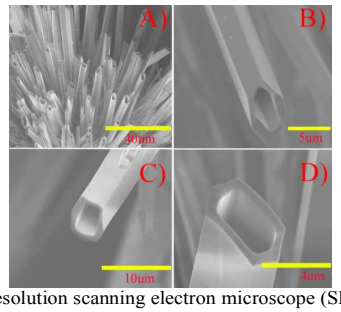

Fig. 1 (A) Low resolution scanning electron microscope (SEM) image of the products, showing a bunch of Gaq_3 sub-microtubes with uniform size. (B, C and D) High resolution SEM images of Gaq_3 sub-microtubes with hexagonal hollow structures and square-like cross-section. The thickness of these tubes is at the nanoscale.

Basically, there are three types of interactions during the growth process, the donor-acceptor (D-A) dipole-dipole interaction, the hydrogen bonding, and the van der Waals interaction. The D-A interaction is much stronger than the latter two, driving significantly the adjacent Gaq_3 molecules in the liquid phase to form sub-microtubes via a self-assemble process. [3,12,41] This process occurs in three steps: (1) formation of seed crystals and aggregation to a regularly hexagonal pad; (2) pad growth accompanying by etching or dissolution at its center, and (3) gradual formation of Gaq_3 tubes, as roughly depicted in the schematic diagram (Fig. S4†)

In the beginning, when injecting the Gaq_3 solution onto the Si substrates, a sudden change of the environment around the Gaq_3 molecules drives the molecules to segregate from the mixture solvent until the seed crystals form, as the adjacent Gaq_3 molecules or clusters can migrate and aggregate due mainly to the D-A interaction and slightly to the hydrogen bonding and van der Waals interactions.[3,12] Gradually, it is leading to nucleation with the continuous aggregation of Gaq_3 molecules. The nuclei can grow slowly with the volatilization of the chloroform. When the concentration of Gaq_3 is sufficiently high, then the nuclei grow into a thin hexagonal pad (Fig. 2A) forms, acting as a building block unit for the Gaq_3 tubes (see Fig. S4†). It should be pointed out that during this process, etching or dissolution at the pad center can occur because the density of defects is high (see Fig. 2B), a phenomenon observed during the growth of [2-(p-dimethylaminophenyl)ethenyl]phenylmethylenepropanedinitrile (DAPMP) crystalline microtubes.[37] In addition, a concave area forms at the pad center (see Fig. 2B), whereas the outmost surface of this pad remains very smooth (see Fig. 2B and 2C). Later on this hexagonal building block unit continues to grow thicker and thicker along the growth c-axis of α-Gaq_3.[42,43] In our work, the thickness of this pad changes slowly from ~22 nm (Fig. 2A) to ~260 nm (Fig. 2C). Eventually, sub-microtubes with a wall thickness at the nanoscale form when removing the solvent two days later. In fact, the migration of Gaq_3 molecules are involved in the whole process during the formation of the Gaq_3 tubes. However, the detailed kinetic process of Gaq_3 molecules need further investigation, especially in step 2 and 3.

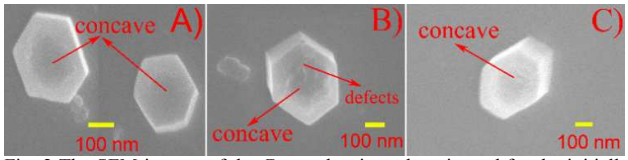

Fig. 2 The SEM images of the Gaq_3 sub-microtubes ripened for the initially stages. (A) A thin hexagonal pad (~22 nm) of the building block unit of the Gaq3 sub-microtubes. (B) The hexagonal pad with evident defects and

concave at the center. (C) The growth of the hexagonal pad (~260 nm) along the c-axis and gradual formation of the sub-microtubes of Gaq_3.

Since defects are nonuniformly distributed around the pad center, the speed of etching or dissolution varies a lot. This promotes the formation of tube-in-tube Gaq_3 sub-microtubes (Fig. 3A) and other tubular structures that have a nanorod at their centers (Fig. 3B).

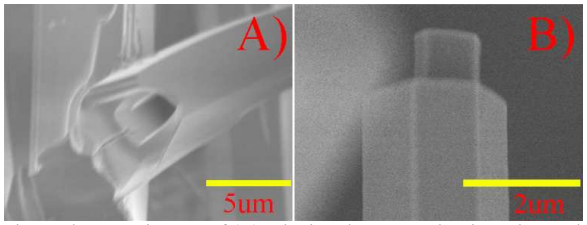

Fig. 3 The SEM images of (A) tube-in-tube Gaq_3 sub-microtubes and (B) a tube with a nanorod inside.

We have also studied the effect of different growth conditions on the formation of Gaq_3 sub-microtubular structures. In particular, we find that controllable growth of other targeting nanostructures can be accomplished through adjustment of temperature and concentration of the Gaq_3 solution. For example, irregular solid instead of hollow sub-microstructures (Fig. S5†) form when the temperature is above 328 K. This is because at high temperature, the volatilization of $CHCl_3$ solvent is faster, leading to a much lower etching or dissolution speed than the self-assembling speed. In addition, at lower temperature ethanol as the poor solvent can reduce the volatility of $CHCl_3$, maintain the solution's liquid nature, and help self-assembling, but it is highly volatile at 328 K, prohibiting formation of tubular nanostructures. Similarly, the concentration of Gaq_3 solution can also be used as an adjusting parameter for controllable growth. By using a Gaq_3 solution with the concentration of 45 mg/ml, we are able to fabricate the Gaq_3 rods (Fig. S6†). However, when the concentration of the Gaq_3 solution is only 10 mg/ml, nonuniform nanostructures are obtained (Fig. S7†). In addition, the grown materials' structures and shapes can also be controlled by ethanol. This is confirmed by the fact that Gaq_3 rods rather than tubes are made in the absence of ethanol and the concentration of the Gaq_3 solution is 36 mg/ml (Fig. S8†).

The shapes and structures of materials can significantly affect their functional properties, allowing optimizing materials for practical applications through controllable growth of materials with different shapes and structures. In order to investigate the functional prospects of these newly synthesized tubes, we have measured their optical properties by photoluminescence (PL) spectroscopy. As shown in Fig. 4A, the PL spectrum exhibits a major peak at 538 nm (2.30 eV), attributed to transitions from singlet (S_1) to ground state (S_0).[45,46] Going from this peak position to either longer or shorter wavelength, the change of intensity is very symmetric for a broad range of light wavelengths between 400 nm and 800 nm, a feature in good agreement with literature.[43,47] Following the relation between absorption coefficient and band gap, $\alpha(h\nu)=A(h\nu-E_g)^{1/2}$,[28] the absorption spectrum analysis (Fig. 4B) shows that the optical band gap of this material is 2.75 eV (inset of the Fig. 4B), a bit smaller than those of Gaq_3 (2.80 eV) and Alq_3 (2.86 eV) films.[28] The tail in the absorbance for the light wavelength between 450 nm and 460 nm arises from the $S_0 \rightarrow S_1$ transitions.[44,45] These measurements show that these tubes preserve the basic optical properties of Gaq_3 while having the advantages of a greater tunability and a larger surface-volume ratio.

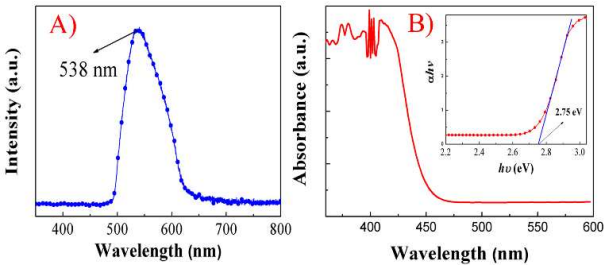

Fig. 4 (A) The photoluminescence spectrum of as-prepared Gaq_3 sub-microtubes at room temperature. (B) The UV−vis absorption spectrum of Gaq_3 sub-microtubes. The inset shows the plot of $(\alpha h\nu)^2$ with respect to photo energy E for the Gaq_3 sub-microtubes.

We further corroborate this point by measuring the field-emission performance of these tubes. The result is indicated by the typical J-E curve, where J and E are the current density and electric field. Indeed, the turn-on voltage (8.5 V um^{-1}) of the Gaq_3 sub-microtube-based device is comparable to that based on Alq_3nanorods, but the maximum current density of the former (2.3 mA cm^{-2}) almost doubles that of the latter (1.38 mA cm^{-1}) (Fig. 5).[45] The field-emission characteristic is analyzed using the Fowler–Nordheim (FN) model, as below:[43]

$$\ln(\frac{J}{E^2}) = \ln(\frac{A\beta^2}{\phi}) + (\frac{-B\phi^{3/2}}{\beta})\frac{1}{E}$$

where A and B are constants (A =1.54 × 10^{-6} A eV V^{-2} and B =6.83 ×10^3 V um^{-1} $eV^{-3/2}$), J is current density, E is electric field, Φ is the work function of the emitting sample, and β is field enhancement factor. The line corresponding to $\ln(J/E^2)$ with respect to $1/E$ is straight (inset of the Fig. 5), indicating that the measured current is indeed from field emission.[4] It also shows the corresponding FN plot of the Gaq_3 sub-microtubes, in which two approximately straight lines are separated at the corresponding threshold fields were observed. This suggests that the field emission from the Gaq_3 sub-microtubes can be described well by the FN theory, but the parameters at low and high fields are different.[4,43,47] Even though β is reduced at high field, a larger intercept of the high-field line can be induced by dramatically increasing active emitters.[4] At low-field, the protuberances in tube tips or edges serve as the main electron emitters, because electrons emitting from a sharper tip are easier.[4]

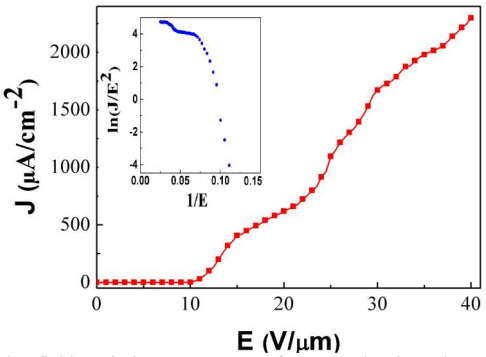

Fig. 5 The field emission J-E curve of Gaq_3 sub-microtubes with the corresponding FN plot shown in inset.

Conclusions

In conclusion, we have successfully synthesized Gaq_3 sub-microtubes with wall thickness at the nanoscale by using an extremely facile solution approach. Formation of these sub-microtubes is accomplished through self-assembling, which is controllable by adjusting experimental condition. Furthermore, this new type of structures possess comparable optical properties to other nanostructures, but they have a greater tunability and a bigger surface-volume ratio, allowing them particularly useful for optoelectronic applications. In particular, device based on these new tubular structures exhibits outstanding field emission performance, mostly evident from a relatively low turn-on voltage but a very high maximum current density. This controllable growth mechanism is highly transferrable to growing other organic nanomaterials with desired shapes and structures.

Acknowledements

The authors are grateful for financial support from the Natural Science Foundation of China (61176019, 11374184, 11444007, and 61106083).

Notes and references

1 C. M. Jiang and J. H. Song, Small, 2014, **10**, 5042-5046.

2 F. PelayoGarcía de Arquer, A. Mihi and G. Konstantatos, Nanoscale, 2015, **7**, 2281-2288.

3 W. Chen, Q. Peng and Y. D. Li, Adv. Mater., 2008, **20**, 2747-2750.

4 G. Xu, Y. B. Tang, C. H. Tsang, J. A. Zapien, C. S. Lee and N. B. Wong, J. Mater. Chem., 2010, **20**, 3006-3010.

5 Q. H. Cui, Y. S. Zhao and J. N. Yao, Chem. Sci., 2014, **5**, 52-57.

6 Y. Liu, N. Wei, Q. L. Zhao, D. H. Zhang, S. Wang and L. M. Peng, Nanoscale, 2015, **7**, 6805-6812.

7 P. Avouris, M. Freitag and V. Perebeinos, Nat. Photon., 2008, **2**, 341-350.

8 J. C. Charlier, X. Blase and S. Roche, Rev. Mod. Phys., 2007, **79**, 677-732.

9 A. H. Liang, G. Y. Shang, L. L. Ye, G. Q. Wen, Y. H. Luo, Q.Y. Liu, X. H. Zhang and Z. L. Jiang, RSC Adv., 2015, **5**, 21326-21331.

10 S. J.Soenen, W. J. Parak, J. Rejman and B. Manshian, Chem. Rev., 2015, **115**, 2109-2135.

11 M. B. Gawande, S. N. Shalke, R. Zboril and R. S. Varma, Acc. Chem. Res., 2014, **47**, 1338-1348.

12 Y. S. Zhao, W. S. Yang, D. B. Xiao, X. H. Sheng, X. Yang, Z. G. Shuai, Y. Luo and J. N. Yao, Chem. Mater., 2005, **17**, 6430-6435.

13 T. Shimizu, H. Minamikawa, M. Kogiso, M. Aoyagi, N. Kameta, W. X. Ding and M. Masuda, Polym. J., 2014, **46**, 831-858.

14 A. G. Cheetham, P. Zhang, Y-an. Lin, L. L. Lock and H. G. Cui, J. Am. Chem. Soc., 2013,**135**, 2907-2910.

15 M. M. Henricus, K. T. Johnson and I. A. Banerjee, Bioconjugate. Chem., 2008, **19**, 2394-2400.

16 T. Tanaka and A. Osuka, Chem. Soc. Rev., 2015, **44**, 943-969.

17 N. Goubet, I. Tempra, J. Yang, G. Soavi, D. Polli, G. Cerullo and M. P. Pileni, Nanoscale, 2015, **7**, 3237-3246.

18 M. Muccini, M.A. Loi, K. Kerevey and R. Zamboni, Adv. Mater. 2004, **16**, 861-864.

19 P. E. Burrows, L. S. Sapochak, D. M. McCarty, S. R. Forrest and M. E. Thompson, Appl. Phys. Lett. 1994, **64**, 2718-2720.

20 D. L. Sun, L. F. Yin, C. J. Sun, H. W. Guo Z. Gai, X. G. Zhang, T.Z. Ward, Z. H. Cheng and J. Shen, Phys. Rev. Lett. 2010, **104**, 236602-1.

21 E. Madan, R. Gogna, B. Keppler and U. Pati, Plos One 2013, **8**, 1-8.

22 M. A. Jakupee, M. Galanski, V. B. Arion, C. G. Hartinger and B. K. Keppler, Dalton Trans. 2008, 183-194.

23 L. S. Foteeva, N. V. Stolyarova and A. R. Timerbaev, J. Pharmaceut. Biomed. 2008, **48**, 218-222.

24 Z. G. Yin, B. X. Wang, G. H. Chen and M. J. Zhan, J. Mater. Sci. 2011, **46**, 2397-2409.

25 F. F. Muhammad and K. Sulaiman, Mater. Chem. Phys. 2014, **148**, 473-477.

26 Y. W. Yu, C. P. Cho and T. P. Perng, Nanoscale Res. Lett. 2009, **4**, 820-827.

27 M. Brinkmann, B. Fite, S. Pratontep and C. Chaumont, Chem. Mater. 2004, **16**, 4627-4633.

28 F. F. Muhammad, A. I. A. Hapip and K. Sulaiman, J. Organomet. Chem. 2010, **695**, 2526-2531.

29 A. V. Rudnev, L. S. Foteeva, C. Kowol, R. Berger, M. A. Jakupec, V. B. Arion, A. R. Timerbaev and B. K. Keppler, J. Inorg. Biochem. 2006, **110**, 1819-1826.

30 A. R. Timerbaev, Metallomics 2009, **1**, 193-198.

31 D. G. Filatova, I. F. Seregina, L. S. Foteeva, V. V. Pukhov, A. R. Timerbaev and M. A. Bolshov, Anal. Bioanal. Chem. 2011, **400**, 709-714.

32 J. K. Abramski, L. S. Foteeva, K. Pawlak, A. R. Timerbaev and M. Jarosz, Analyst 2009, **134**, 1999-2002.

33 M. Brinkmann, B. Fite, S. Pratontep and C. Chaumont, Chem. Mater. 2004, **16**, 4627-4633.

34 F. F. Muhammad and K. Sulaiman, Materials Chemistry and Physics, 2014, **148**, 473-477.

35 Y. W. Yu, C. P. Cho and T. P. Perng, Nanoscale Res. Lett., 2009, **4**, 820-827.

36 J. P. Zhang and G. Frenking, Chem. Phys. Lett., 2004, **394**, 120-125.

37 J. S. Hu, Y. G. Guo, H. P. Liang, L. J. Wan and L. Jiang, J. Am. Chem. Soc. 2005, **127**, 17090-17095.

38 X. J. Zhang, X. H. Zhang, W. S. Shi, X. M. Meng, C. S. Lee and S. T. Lee, Angew. Chem. Int. Ed. Engl. 2007, **46**, 1525-1528.

39 L. X. Lin, L. Ma, S. W. Zhang, J. T. Huang and D. A. Allwood, Cryst. Eng. Comm. 2015, **17**, 1491-1495.

40 S. J. Fang, Z. H. Pang, L. Lin, F. G. Wang, W. F. Zheng, Y. H. Li, Y. Dai and S. H. Han, Physica E 2011, **43**, 1470-1474.

41 H. Z. Wang, X. G. Zheng, W. D. Mao, Z. X. Yu, and Z. L. Gao, Appl. Phys. Lett. 1995, **66**, 2777-2779.

42 C. P. Cho, C. A. Wu and T. P. Perng, Adv. Funct. Mater. 2006, **16**, 819-823.

43 J. S. Hu, H. X. Ji, A. M. Cao, Z. X. Huang, Y. Zhang, L. J. Wan, A. D. Xia, D. P. Yu, X. M. Meng and S. T. Lee, Chem. Commun. 2007, **29**, 3083-3085.

44 J. W. Bai, P. Chen, Y. L. Lei, Y. Zhang, Q. M. Zhang, Z. H. Xiong and F. Li, Org. Electron. 2014, **15**, 169-174.

45 M. Cölle and C. Gärditz, Appl. Phys. Lett. 2004, **84**, 3160-3162.

46 A. M. Collins, S. N. Olof, J. M. Mitchels and S. Mann, J. Mater. Chem. 2009, **19**, 3950-3954.

47 J. J. Chiu, C. C. Kei, T. P. Perng and W. S. Wang, Adv. Mater. 2003, **15**, 1361-1364.